Use of eddy current testing method in detection and evaluation of sensitisation and intergranular corrosion in austenitic stainless steels

Article *in* Corrosion Science · June 2006

DOI: 10.1016/j.corsci.2005.05.017

CITATIONS
92

READS
2,643

9 authors, including:

Hanefan Shaikh
ilma university
46 PUBLICATIONS **960** CITATIONS
SEE PROFILE

B. Sasi
Indira Gandhi Centre for Atomic Research
33 PUBLICATIONS **375** CITATIONS
SEE PROFILE

Anita Toppo
Indira Gandhi Centre for Atomic Research
29 PUBLICATIONS **562** CITATIONS
SEE PROFILE

Purna Chandra Rao Bhagi
Indira Gandhi Centre for Atomic Research
274 PUBLICATIONS **2,015** CITATIONS
SEE PROFILE

Available online at www.sciencedirect.com
SCIENCE DIRECT®
Corrosion Science 48 (2006) 1462–1482
CORROSION SCIENCE
www.elsevier.com/locate/corsci

Use of eddy current testing method in detection and evaluation of sensitisation and intergranular corrosion in austenitic stainless steels

H. Shaikh [a,*], N. Sivaibharasi [a], B. Sasi [b], T. Anita [a], R. Amirthalingam [c], B.P.C. Rao [b], T. Jayakumar [b], H.S. Khatak [a], Baldev Raj [d]

[a] *Corrosion Science and Technology Division, Indira Gandhi Center for Atomic Research, Kalpakkam 603 102, Tamil Nadu, India*
[b] *Division for Post Irradiation Examination and Non Destructive Testing, Indira Gandhi Center for Atomic Research, Kalpakkam 603 102, Tamil Nadu, India*
[c] *Department of Physics, Government Arts College, Cuddalore 607 001, Tamil Nadu, India*
[d] *Indira Gandhi Center for Atomic Research, Kalpakkam 603 102, Tamil Nadu, India*

Received 7 October 2004; accepted 23 May 2005
Available online 10 August 2005

Abstract

This paper deals with the applicability of eddy current testing (ECT) technique to assess and quantify sensitisation and intergranular corrosion (IGC) in thermally aged AISI type 316 stainless steel. Chemical and electrochemical tests specified by ASTM A262 Practices A and E (Strauss test) and G108, and ECT, were used to quantify degree of sensitisation (DOS). The DOS was categorised based on severity of the crack after bend test in increasing order as unaffected, fissured, cracked, and broken. The eddy current (EC) amplitude increased with increasing DOS in both the as-aged and Strauss tested conditions. The EC amplitude in as-aged condition was smaller than in Strauss tested condition. Empirical relationships were established between ECT amplitude and other DOS parameters.

* Corresponding author. Tel.: +91 4114 280121; fax: +91 4114 280081/280060/280301.
E-mail address: hasan@igcar.ernet.in (H. Shaikh).

0010-938X/$ - see front matter © 2005 Elsevier Ltd. All rights reserved.
doi:10.1016/j.corsci.2005.05.017

Keywords: Austenitic stainless steel; Sensitisation; Intergranular corrosion; Strauss test; Eddy current testing; Electrochemical potentiokinetic reactivation technique

1. Introduction

The periodic inspections of structural materials and components in plants are very important to detect and evaluate their degradation. The stringent inspection regulations necessitate the use of more advanced and reliable non-destructive testing (NDT) methods for assessing structural integrity of parts, specifically to detect the damage at its initiation stage, in other words, much before the defects detected by conventional NDT techniques. The structural integrity of the components is affected by various types of material degradation processes including intergranular corrosion (IGC), pitting corrosion, thinning, creep and fatigue damage. Among various structural materials, austenitic stainless steels are most commonly used in a wide variety of industries including power, chemical, petrochemical, process and nuclear. These steels exhibit excellent resistance to general corrosion, adequate mechanical properties and good fabricability. However, these steels suffer from attack by localised corrosion, such as pitting corrosion, crevice corrosion, intergranular corrosion (IGC) and environment-induced cracking. A number of failures of stainless steel components have been attributed to these localised corrosion processes, particularly to IGC/intergranular stress corrosion cracking (IGSCC), in nuclear and petrochemical industries [1]. Most of these failures have been attributed to sensitisation of austenitic stainless steels [2].

Sensitisation of austenitic stainless steel occurs when heated or cooled slowly, as in welding, or during isothermal exposure during service, in the temperature range of 723–1123 K. During this high temperature exposure, depletion of Cr to less than 12% occurs in the region adjacent to the grain boundary due to the precipitation of a continuous network of chromium-rich $M_{23}C_6$ carbides. In molybdenum containing austenitic stainless steel, these chromium-rich $M_{23}C_6$ carbides also contain molybdenum, thus causing a depletion of Cr + Mo in the grain boundary region during sensitisation [3]. When sensitised austenitic stainless steel is exposed to a corrosive environment, the chromium depleted regions dissolve, leading to IGC. The probability of the heat-affected zone (HAZ) being sensitised during welding would depend on the time it spends in the sensitisation temperature range. The residence time spent by the HAZ in this temperature range depends on the welding heat input, which, in turn, governs the heating and cooling rates. Lower heat input processes are beneficial from sensitisation point of view due to the faster cooling rates through the sensitisation temperature regime.

The kinetics of $M_{23}C_6$ precipitation, and, hence, the resultant DOS could be predicted from a time–temperature-sensitisation (TTS) diagram [4]. However, these curves represent sensitisation during isothermal heat treatments. Sensitisation during continuous cooling, as in welding, can be predicted by means of a continuous cooling sensitisation (CCS) diagram [5]. The susceptibility of a stainless steel to sensitisation

is very strongly influenced by its chemical composition. Decreasing carbon content, and increasing nitrogen, manganese, chromium and molybdenum contents, improve the resistance to sensitisation [6–9]. Composition based correlations have been derived to predict time required for sensitisation [10]. Effective chromium contents, Cr^{eff}, calculated based on compositions, suggested that, for types 304/304L stainless steels, a Cr^{eff} of 14.0 and above ensured resistance to IGC in nitric acid applications, and a Cr^{eff} of 13.5 and above ensured IGC resistance in accelerated Strauss test [11]. Metallurgical factors also significantly influence the kinetics and DOS in austenitic stainless steels. Increasing grain size and cold work reduce the resistance to sensitisation [8,9,12,13].

ASTM standardised tests are used to evaluate IGC caused by sensitisation in austenitic stainless steels. These tests are either chemical or electrochemical in nature. ASTM Standard A 262 Practice A to F detail the standards for chemical and metallographic tests to determine IGC in austenitic stainless steels [14]. They are commonly used as qualification/acceptance criteria during purchase/fabrication stage. However, non-inclusion of acceptance limits in these standards leaves the interpretation of results open to users. Besides not quantifying the DOS, these chemical tests are also destructive and slow—a situation that is not welcome at plant site. The most often used chemical technique is the ASTM A262 Practice E test, popularly known as the Strauss test, that is used as qualification check. The test recommends a bend test after exposure to $Cu–CuSO_4–H_2SO_4$ test medium to qualify the material. However, the bend test does not give any quantitative value for the DOS. Electrical resistivity and tensile properties are changed considerably by the intergranular attack in the Strauss test medium [14]. Hence the changes in these properties can be used to quantify the DOS after exposure to the Strauss test solution [15]. To overcome these limitations of chemical tests, an electrochemical technique, known as electrochemical potentiokinetic reactivation (EPR) technique, was developed by Cihal [16], Novak et al. [17] and Clarke et al. [18]. This technique is a quantitative, non-destructive and rapid method, which is essentially suitable for field use. This technique was standardised by ASTM to quantify the DOS in AISI types 304 and 304L stainless steels [19]. The EPR technique has been successfully used to quantify the DOS in other stainless steels, alloy 800 and Ni base alloys [20–22]. Two versions of the EPR technique are practiced today, viz. the single loop technique and the double loop technique [15]. Double loop technique has advantage over single loop technique in that it automatically compensates for changes in alloy composition, and in that the surface finish is not very critical, which makes it an automatic choice for on-field applications. Reactivation charge, ratio of reactivation to activation charge, peak reactivation current density, ratio of peak current densities on reactivation to activation are some of the parameters used to quantify the DOS.

Though the EPR technique provides a criterion for identifying the complete absence of sensitisation and, thus, is useful in quality control of fabricated components, it does not readily provide an acceptance criteria if a certain DOS is present in the material. Many studies in literature have attempted comparison of DOS measured using EPR technique with that determined by more established practices [16–18,21], but very few of these are quantitative [16,18]. Despite all these efforts, EPR

technique has not shown much promise as a tool for quantifying DOS. This is because of its high sensitivity to the changes in chemical compositional of the stainless steels e.g., two alloys with different chemical composition but with the same DOS need not give the same reactivation ratio. Secondly, inconsistencies exist in the correlation between ASTM A262E and EPR DOS results due to effects of temperature, which does not permit a threshold DOS to be defined. These drawbacks in the EPR technique calls for applying some other conventional NDT technique to unambiguously quantify DOS.

The doubt over the application of EPR technique to quantify threshold DOS for IGC in austenitic stainless steels calls for development of some other NDT techniques for assessing the DOS. In addition, this could develop into a powerful tool to monitor the component for the effects of high temperature service, including in-service sensitisation, during shutdowns. ECT presents a viable alternative as it can sense the changes in electrical conductivity/permeability associated with chromium depletion and $M_{23}C_6$ precipitation and also microcracking. ECT is a versatile NDT technique for detection of defects, microstructural variations and corrosion in electrically conducting materials, such as stainless steel. This method uses the principles of electromagnetic induction to inspect electrically conducting components. In ECT, an alternating current is made to flow in a coil (called probe), which, in turn, produces an alternating magnetic field around it. This coil, when brought close to the electrically conducting material surface being inspected, induces EC into the material. These EC, in turn, generate an alternating magnetic field which may be detected either as a voltage across a second coil or by the perturbation of the impedance of the original coil. The EC are generally parallel to the direction of coil winding. The depth of penetration of EC is controlled by skin effect, which depends on electrical conductivity, magnetic permeability and frequency of excitation. The presence of defects such as cracks, thickness loss or any other discontinuities in the material, disrupt the EC flow. Apart from these defects, a number of variables such as changes in material conductivity and permeability (through microstructural/substructural changes), wall thickness and surface roughness influence the EC distribution in materials [23]. Shaikh et al. studied the applicability of ECT to detect sensitisation in weldments of AISI type 316L stainless steels [24]. In this study, characterisation by ECT of the base metal indicated that in the as-aged condition, no variation in EC amplitude with increasing aging time was observed. This suggested that ECT could not detect sensitisation. However, after exposure to $Cu–CuSO_4–H_2SO_4$ solution, EC amplitudes of aged base metals dramatically increased, thus implying that ECT could be used to detect and quantify IGC. The results of ECT technique correlated well with the findings of the EPR and bend tests. In the case of weld metal, the EC amplitude decreased significantly with increasing aging time in as-aged condition, thus indicating the applicability of ECT to detect transformation of δ-ferrite to σ phase. However, unlike in the base metal, the EC amplitudes after exposure of the weld metal to $Cu–CuSO_4–H_2SO_4$ solution did not vary much, thus confirming that the extent of Cr-depletion was not significant enough to cause IGC in the weld metal.

In the present laboratory-based study, an attempt has been made to quantify DOS and IGC in AISI type 316 stainless steel by the eddy current testing technique. Based

on the response to ASTM A262 Practice E and the EPR tests, the IGC failure was categorised into four types and the ECT response for each type was demarcated. Such a demarcation of the EC signal would be very useful to gauge the extent of sensitisation during post-fabrication (hot forming, welding, stress relieving, etc.) inspection of components such as dished end or during in-service inspection of the component. Emperical relations were established correlating the EC signal amplitude, EPR ratio of charge and depth of attack.

2. Experimental procedures

AISI type 316 stainless steel (chemical composition in Table 1) plates of 3 mm thickness were heat treated at 873, 973 and 1073 K for different time durations in the range of 15 min to 25 h. Rectangular specimens of dimensions $100 \times 10 \times 3$ mm were then machined from the as-received and aged material.

Optical microscopic examination of the as-received and aged base metals was carried out after etching (i) electrolytically in 10% (by weight) ammonium persulphate solution at a current density of 1 A/cm^2 for 1.5 min to detect intergranular carbide precipitation, and (ii) in modified Murakami reagent (20 g potassium hydroxide and 20 g potassium ferricyanide in 100 ml water) at 368 K to detect σ phase precipitation.

The as-received and aged specimens were tested for IGC resistance by the ASTM A262 Practice E test (modified Strauss test) by embedding the rectangular specimens in copper chips and then exposing them to a boiling 16% H_2SO_4 solution containing 100 g/L of $CuSO_4 \cdot 6H_2O$ for 24 h. The rectangular strips were removed and bent through 180°. The bent surfaces were then examined for cracks in a stereomicroscope at a magnification of 5×. EPR tests were carried out on the as-received and aged specimens in a solution containing 0.5 M H_2SO_4 + 0.01 M NH_4SCN at room temperature, using the double loop technique. The polarisation scan was carried out at the rate of 6 V/h in both the forward and reverse directions. The forward scan was carried out after holding the specimen at −300 mV vs saturated calomel electrode (SCE) for 2 min. The reverse scan was carried out after holding the specimen at +200 mV (SCE) for 2 min. The charges and peak current densities for passivation during forward (activation) scan and reverse (reactivation) scan were compared to quantify the DOS.

The DOS in the as-received and aged specimens was also measured using the ECT technique. The measurements were made on as-aged specimens and after exposure to Strauss test solution. An eddy current instrument (Model ECT 3300 supplied by M/s. Eddy Current Technology Inc., USA) with a surface absolute eddy current probe (diameter 5 mm) was used for this investigation. The test parameters such as fre-

Table 1
Chemical composition of AISI type 316 stainless steel

Element	C	Cr	Ni	Mo	Mn	Si	P	S
Concentration (wt.%)	0.055	18.0	11.8	2.3	1.7	0.45	0.067	0.027

quency, phase and gain were optimised using a reference specimen that was not subjected to ageing treatment. The lift-off (distance between specimen and ECT probe) signal for the reference specimen was rotated such that it became parallel to the real component of impedance. The test frequency was chosen such that maximum impedance change occurred for small changes in material conductivity/permeability that was attributed to sensitisation as well as to IGC. To achieve this, the set of frequencies with different depth of investigation (skin effect) in the range of 0.5–2.1 mm in the specimens were chosen and the optimum frequency was arrived at. The EC response at different test frequencies and depth of penetration for an as-aged specimen (973 K/0.5 h) is shown in Fig. 1. The frequency response reached a maximum at 160 kHz and the depth of penetration of EC at this frequency was about 1.0 mm. In view of this, 160 kHz was chosen as the optimum testing frequency. The other optimised EC instrument parameters followed in the investigations were phase angle of 49° and a gain of 36 dB. The typical experimental setup is shown in Fig. 2. In order to assess the DOS and IGC, the EC response from every specimen was measured at a number of

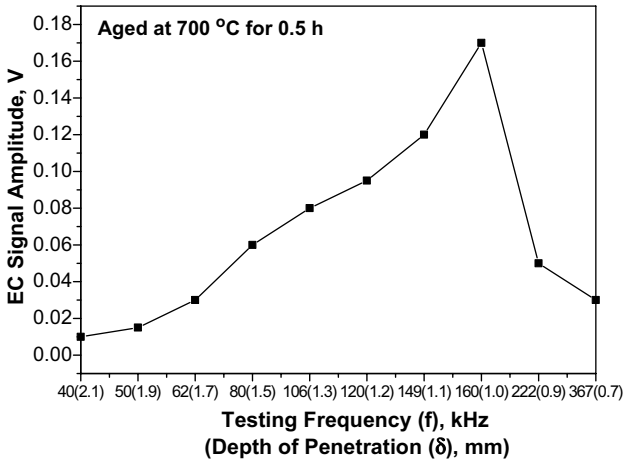

Fig. 1. Optimisation of test frequency. At 160 kHz ($\delta = 1$ mm), the EC response shows a distinct peak.

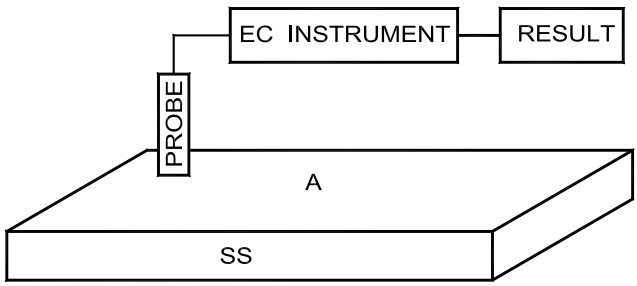

Fig. 2. Experimental setup used for corrosion studies in stainless steels.

locations and the averaged data was taken for each measurement. The analogue output from the probe was converted into a digital signal using analog to digital converter and then stored on computer for analysis.

3. Results and discussion

Monitoring of a component for any degradation by IGC is of paramount importance during high temperature service since increasing susceptibility to IGC indicates increasing propensity of the stainless steel to pitting corrosion and IGSCC. The degradation of corrosion properties of austenitic stainless steels could be extremely severe if Cr and Mo get depleted in localised regions rather than uniformly [6,7]. A sensitised HAZ is detrimental to the integrity of the weld joint in service since it is the weakest link in a weld joint from SCC point of view [25]. Muraleedharan et al. reported that for a given EPR charge value, the IGSCC susceptibility decreased with increasing ageing temperature [26]. The following discussions deal at great length the possibility of using eddy current testing technique. Emperical relations have been developed linking the ECT, EPR and optical results.

3.1. Assessment of degree of sensitisation (DOS) by ASTM A262 Practice E

The results of ASTM A262 Practice A and Practice E (bend tests) on aged type 316 stainless steel are detailed in Table 2. Bend test was used as a criterion to categorise the DOS, which was then correlated to values of EPR parameters and EC amplitude. Practice E exposure of aged stainless steel led to dissolution of the Cr-depleted regions. The dissolution of Cr-depleted regions occurred only when there is a total loss of local passivity in these regions. This was possible when the Cr content in those local regions fell to below that required for stainlessness in austenitic stainless steels i.e., <12% Cr. This dissolution led to the formation of microscopic grooves, which acted as stress concentration sites during bend or tensile tests, both of which can be used as per ASTM A262 Practice E. A narrow and deep groove acted as a more efficient stress raiser vis-à-vis a wider and shallow groove. The stress concentration ahead of the microscopic grain boundary groove resulting from dissolution of Cr-depleted regions caused the cracking on the outside of the bend.

In the present study, low magnification optical microscopic examination of the bent region was used to classify the Practice E exposed aged specimens into four categories viz. unaffected base metal (Fig. 3(a)), base metal containing fissures (Fig. 3(b)), base metal containing cracks (Fig. 3(c)) and broken base metal (Fig. 3(d)). Based on this classification the results of the EPR and EC tests were analysed.

3.2. Microstructural examination

The results of microstructural examination of specimens with various DOS are depicted in Fig. 4(a)–(e). For specimens that were broken or contained cracks after Strauss test, a completely ditched structure due to continuous grain boundary $M_{23}C_6$

Table 2
Eddy current responses from various aged specimens

No.	EPR results I_r/I_a (%)	EPR results Q_r/Q_a (%)	Depth of attack (μm)	EC response (V)		Category of the specimen (after bend test)
				As-aged specimen	Strauss tested specimen	
1	0.02	0.16	–	0.0	0.0	Not affected
2	0.27	0.18	–	0.012	0.12	Not affected
3	0.25	0.17	–	0.012	0.13	Not affected
4	0.24	0.18	–	0.012	0.12	Not affected
5	0.011	0.17	–	0.012	0.13	Not affected
6	0.011	0.15	–	0.012	0.12	Not affected
7	0.009	0.22	–	0.012	0.12	Not affected
8	0.29	0.04	–	0.015	0.27	Not affected
9	0.89	3.95	–	0.17	0.62	Fissures
10	0.92	1.98	–	0.15	0.8	Fissures
11	1.38	0.96	–	0.17	0.82	Fissures
12	0.77	0.45	–	0.15	0.75	Fissures
13	0.52	0.38	–	0.15	0.72	Fissures
14	5.6	5.86	75.0	0.21	2.43	Cracks
15	12.15	17.86	147	0.30	6.22	Cracks
16	5.62	6.18	79.8	0.35	3.18	Cracks
17	18.15	20.01	154	0.40	6.5	Cracks
18	14.2	26.7	104	0.35	6.4	Cracks
19	5.56	12.23	92.1	0.30	4.2	Cracks
20	20.87	36.11	103	0.49	6.7	Cracks
21	56.8	67.2	308	0.65	7.85	Broken
22	37.6	59.1	190	0.62	7.5	Broken

precipitation was observed (Fig. 4(c) and (d)). Fig. 4(b) shows that in specimens containing fissures, a dual structure due to discontinuous grain boundary $M_{23}C_6$ precipitation was observed. Unaged and aged specimens that were unaffected by Strauss test showed two possible types of structures viz. a step structure as in unaged base metal (Fig. 4(a)) and a fully ditched structure (Fig. 4(e)). In the latter case, a fully ditched structure is visible, since the carbides are dissolved in electrolytic etching in ammonium persulphate solution. However, the steel remains unaffected in bend test since the grain boundary Cr-depletion, subsequent to $M_{23}C_6$ precipitation, is self-healed by diffusion of Cr to the grain boundary area from the bulk of the austenite grains.

Examination of the cross-section of the 1 μm finished surfaces (by diamond paste polishing), after exposure to the Strauss test showed grain boundary attack to a certain depth, as shown in Fig. 5. Table 2 shows that the depth of attack by the Strauss test solution increased with increasing DOS.

Etching with modified Murakami reagent reveals the various precipitates in an austenitic stainless steel under an optical microscope by colouring the various precipitates differently, for example, σ phase appears as brick red precipitate, carbides as gray particles, etc. [27]. Optical microscopic examination of specimens after etching with modified Murakami reagent did not show the presence of σ phase. The propensity of austenitic stainless steel to σ phase precipitation has been formulated by Hull

[28]. As per this formulation, an equivalent chromium content (ECC) of above 17.8 wt.% made the steel susceptible to σ phase precipitation. In the present study, the steel had an ECC of 20.14, thus suggesting that it was susceptible to σ embrittlement. But no σ particles were observed on examination under an optical microscope. This could be because the ECC does not account for the effect of a potent σ phase stifler like carbon. Gill et al. [27] proposed a normalised equivalent chromium content (NECC), which is the ratio of ECC to the carbon content of the alloy. The NECC of the steel was 366 as against 540 required for σ phase precipitation, suggesting a low propensity for the steel to undergo σ embrittlement.

3.3. Assessment of degree of sensitisation (DOS) by EPR tests

The EPR tests for quantifying DOS were carried out by the double loop technique because this method automatically compensates for changes in alloy composition

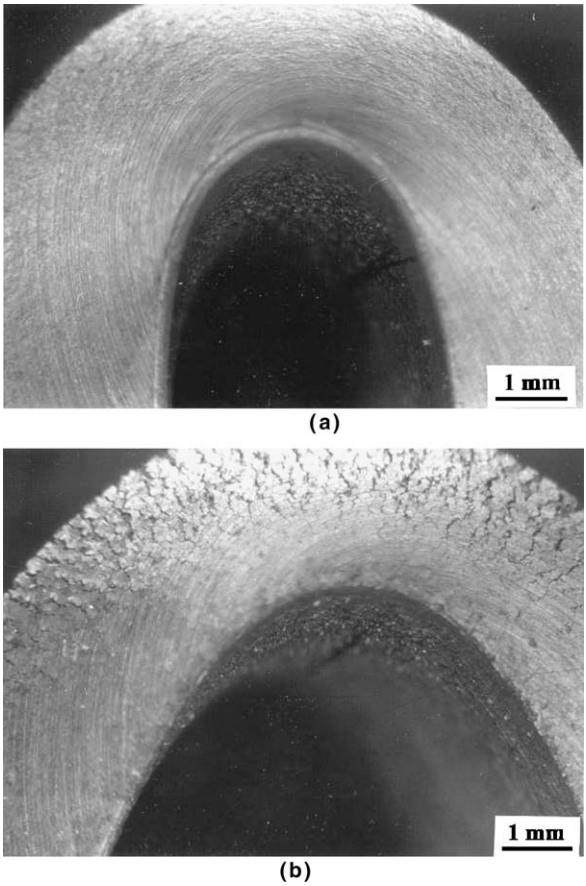

Fig. 3. Classification of the DOS after exposure to Strauss test solution, based on appearance after bend test: (a) unaffected, (b) fissures, (c) cracks, and (d) broken.

(c)

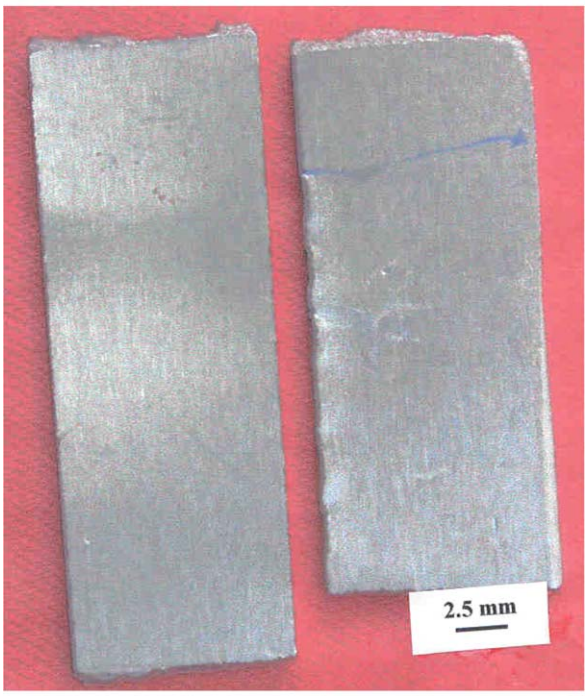

(d)

Fig. 3 (*continued*)

and also for differences in surface finish. The ratios of peak current densities during reactivation (I_r) to activation (I_a) and reactivation charge (Q_r) to activation charge (Q_a) were used as assessment parameters to evaluate DOS. The comparison between the EPR test and the bend test results is shown in Table 2. It is seen that the susceptibility to IGC in Strauss test increases with increasing ratio of Q_r/Q_a and I_r/I_a. At values of Q_r/Q_a greater than 59% and I_r/I_a greater than 37%, the samples broke

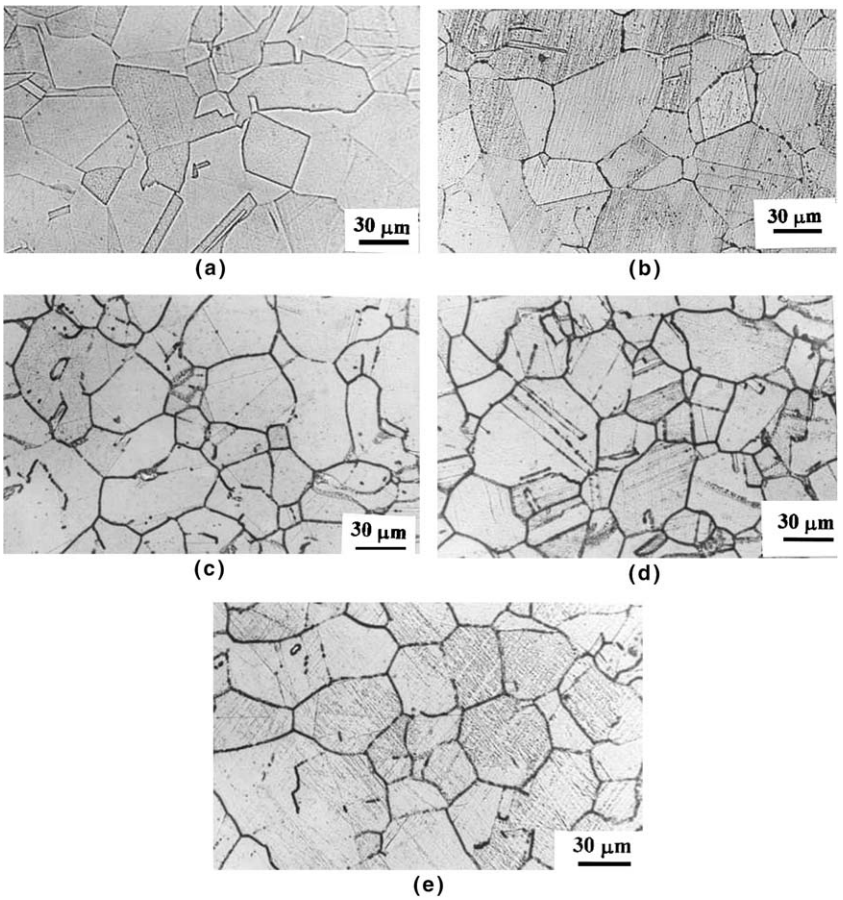

Fig. 4. Microstructures of aged type 316 stainless steel for (a) as-annealed, (b) those which fissured in bend test, (c) those which cracked in bend test, (d) those which broke in bend test, and (e) those which remained unaffected in bend test.

during bend test. The range of values of Q_r/Q_a and I_r/I_a in which (i) cracks were observed in the bend tests were 5.86–36.1% and 5.6–20.8%, respectively, (ii) fissures were observed in the bend test were 0.38–.95% and 0.5–1.4%, respectively. The as-received and unaffected aged specimens after bend test had values of I_r/I_a less than 0.3% and Q_r/Q_a less than 0.2%. As per the standards prepared by International Standards Organisation (ISO) for evaluation of IGC susceptibility by means of double loop EPR test [29], values of $I_r/I_a * 100 > 5$ show medium to strong susceptibility to IGC. Based on this, it can be inferred that the aged specimens that showed fissures or remained unaffected after bend tests were not sensitised.

Fig. 6(a)–(d) represent the EPR results for specimens susceptible to different levels of IGC attack. Fig. 6(c) and (d) show that on activation of aged specimens that showed cracks or got broken on bending after Practice E tests, a shoulder anodic to

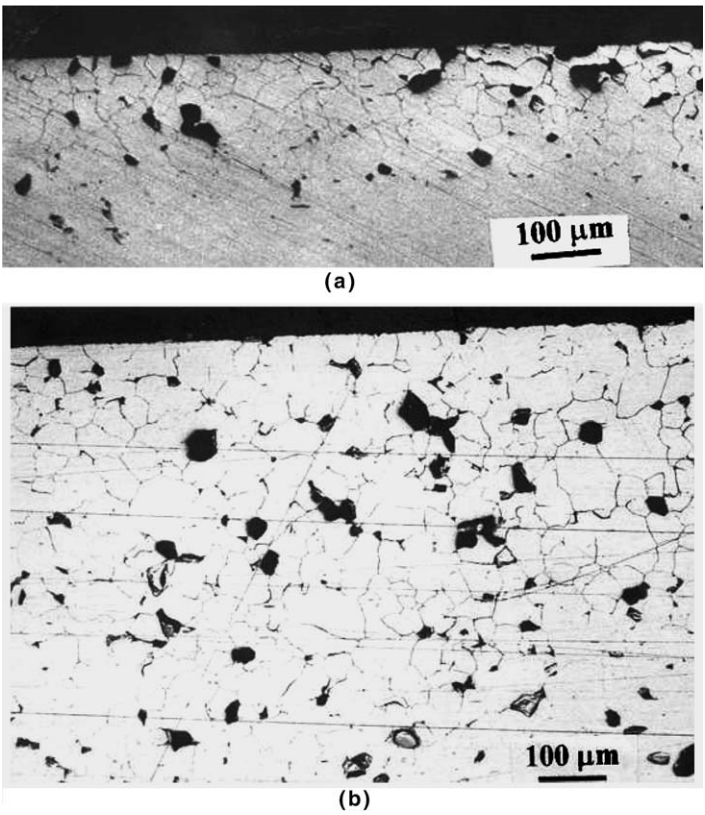

Fig. 5. Micrographs showing depth of attack caused by the Srauss test solution in (a) specimens showing cracks, and (b) in broken specimens.

the main activation peak occurred. However, such a shoulder anodic to the main activation peak was not visible in the material that showed fissures (Fig. 6(b)) or remained unaffected (Fig. 6(a)) on bending after Strauss test. On potentiodynamic scan after activating the specimens at −300 mV, the matrix, Cr + Mo depleted regions at grain boundary and all such artifacts dissolve, giving rise to the activation charge. On holding the potential for 2 min at +200 mV before reactivation, all the artefacts in the grain including the Cr + Mo depleted regions get passivated. On reactivation, only the weaker passive film on the Cr + Mo depleted regions give way leading to dissolution there. Hall and Briant [30] reported an average Mo level of 1.6 wt.% in the depleted region as against the matrix Mo content of 2.5 wt.% in type 316LN stainless steel. The current density of the shoulder nearly corresponded to the peak current density of the reactivation peak, indicating that the shoulder occurred due to dissolution of regions of Cr + Mo depletion. At values of the main peak current density, the whole matrix would passivate. However, regions of Cr + Mo depletion would not undergo complete passivation. At the current density corresponding to the shoulder, the Cr + Mo depleted regions start to passivate. Thus, the occurrence of the shoulder

in activation peak could be related to the difficulty in repassivation of the regions depleted in Cr + Mo, which would necessitate higher potentials for its passivation vis-à-vis the rest of the matrix. Also, the peak current density of the shoulder was higher in the case of broken specimens than cracked specimens. Increasing depletion of Cr + Mo from grain boundary regions caused increased peak current density of the shoulder region in the activation loop. Thus it is seen that the activation scan can also

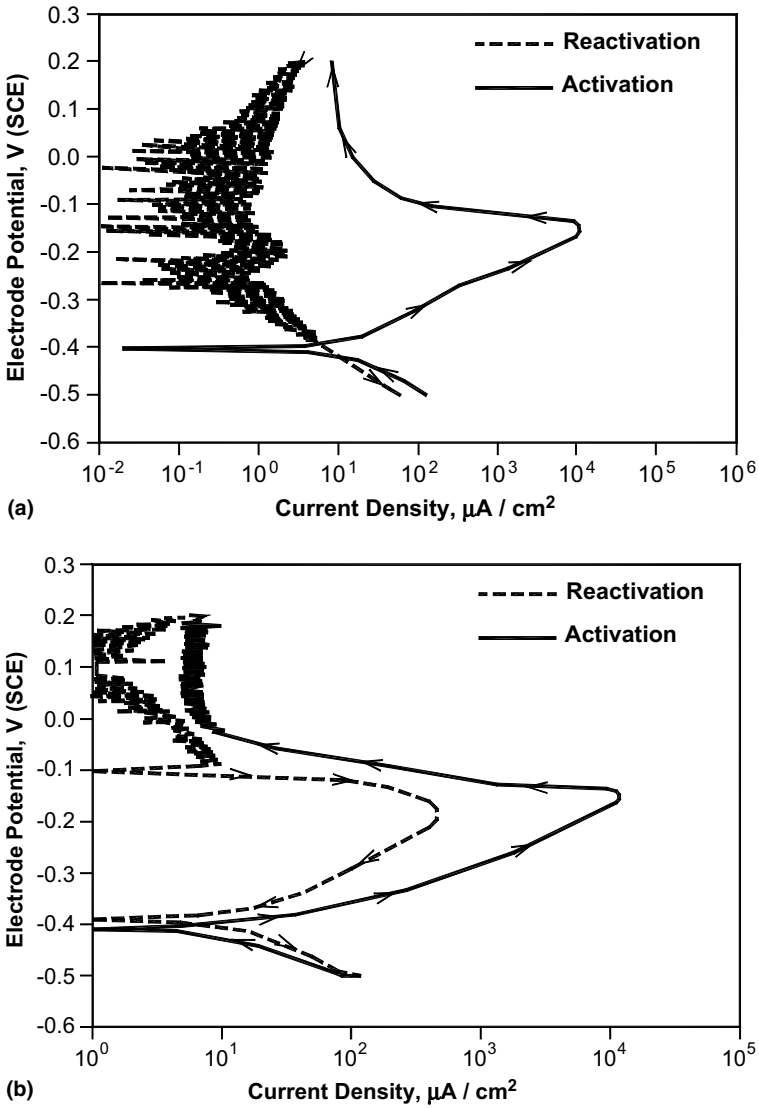

Fig. 6. Double loop EPR curves for type 316 stainless steel that (a) showed no cracking (unaffected), (b) showed fissures, (c) showed cracks, and (d) was broken, in bend tests.

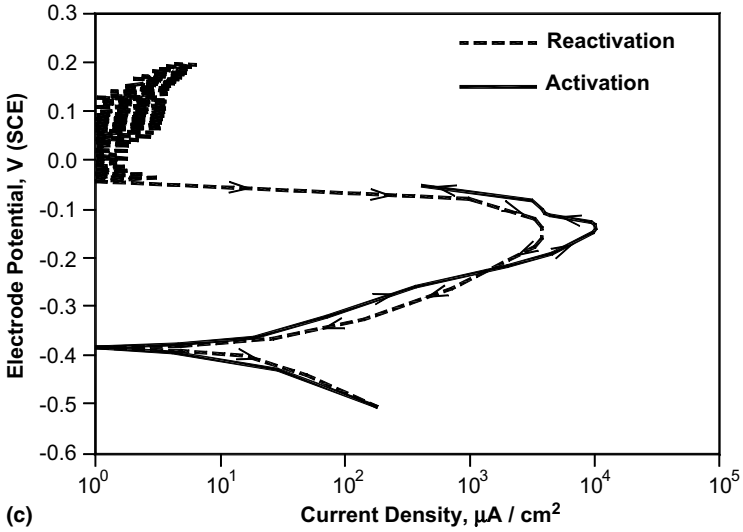

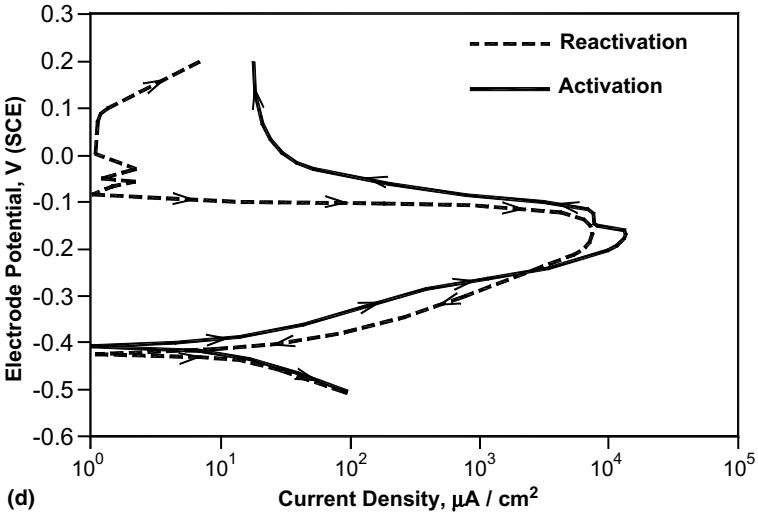

Fig. 6 (*continued*)

give a measure of the DOS in a stainless steel from the value of the peak current density of the shoulder in the activation loop.

The potential at which the peak current density was observed shifted in the noble direction from −178 mV (SCE) in case of samples that showed fissures in bend test to −148 mV (SCE) in case of samples that showed cracking or got broken in the bend test. This observed shift in the peak potentials in the reactivation curves can be attributed to the decrease in the minimum chromium content in the depleted zone [21].

This is in agreement with the reported shift in the anodic peak potential of synthetic FeCrNi alloys with decreasing chromium content [31].

3.4. Assessment of degree of sensitisation (DOS) by eddy current testing

The EC signal amplitudes from various specimens in the as-aged condition (prior to Strauss test) are shown in Fig. 7 and Table 2. It can be seen that the overall change in the amplitude among all the specimens was small i.e., about 0.75 V with a maximum scatter of ±0.008 V. This was attributed to a small change in conductivity/permeability due to depletion of chromium adjacent to grain boundaries which could cause local increase in the nickel content that could result in increased magnetic permeability of the material. A Cr-depleted zone becomes ferromagnetic and its spontaneous magnetisation can be detected [32]. The EC response from the aged specimens after Strauss test is shown in Fig. 8 and Table 2. This figure shows that the overall change in the amplitude among all the specimens was of the order of 8.0 V, much higher than that observed for as-aged specimens. This was attributed to the changes that take place during the Strauss test i.e., dissolution of Cr-depleted regions and the consequent grain boundary grooving. Grain boundary grooving causes enhanced perturbation of EC flow which, in turn, leads to increased impedance change i.e., signal amplitude. As the region of EC probe interrogation is large (nearly 10 mm diameter), the signal amplitude is a superimposed effect of all small localised variations within that region associated with grooving at microscopic level. Fig. 8 clearly shows

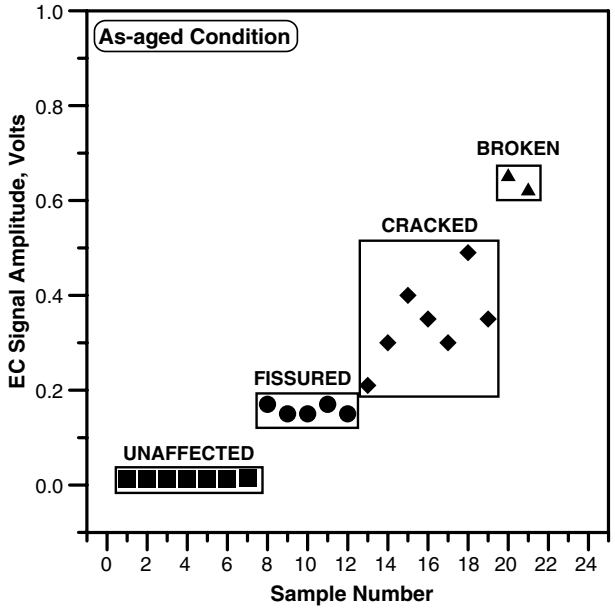

Fig. 7. EC responses from the as-aged condition specimens are in good agreement with the four categories of specimens classified after bend test.

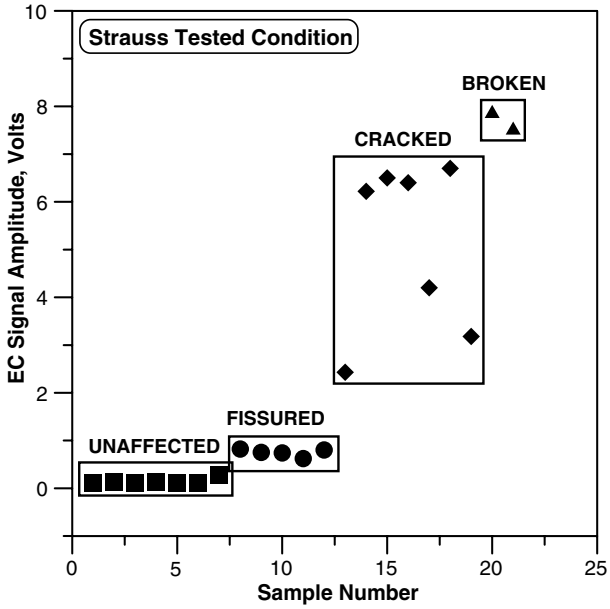

Fig. 8. Comparison of EC responses from the Strauss tested specimens with severity of the cracks developed after bent test.

that in the case of aged specimen exposed to Strauss test, the EC amplitude of the unaffected specimens was less than 0.5 V; for specimen with fissures the EC amplitudes ranged from 0.6 to 0.8 V. The specimens with cracks had EC amplitudes in the range of 2.4–6.7 V while for broken specimens the EC amplitudes ranged from 7.5 to 7.9 V. Repeated measurements at various locations on these specimen found that the scatter was within the range of ± 0.005 V. The fact that unaffected specimens also included those with continuous grain boundary carbide precipitation but self-healed indicated that carbide precipitation per se had little or no role in affecting the conductivity/permeability of the steel. This indicated that the changes in the conductivity/permeability of the as-aged specimens and those exposed to Strauss tests were a consequence of factors related to depletion of alloying elements in the grain boundary region and grain boundary grooving.

From Table 2 it is clearly seen that the EC amplitude values are relatively lower for as-aged specimens in comparison to the corresponding values for Strauss tested specimens, particularly those which experienced fissuring, cracking and breakage. In the case of specimens that have not shown any propensity for IGC, the EC amplitudes are marginally higher in Strauss tested condition in comparison with as-aged condition. Similar studies carried out earlier on AISI type 316L stainless steel specimens (Table 3) revealed that ECT method has accurately predicted the propensity for IGC, as confirmed by Strauss test. However, this propensity for IGC could not be detected effectively by ECT in the as-aged condition (prior to Strauss test). This was attributed to lesser amount of carbide formation and the consequent lesser

Table 3
The range of EC response obtained from the specimens in four category

Range of EC amplitude among various specimen (V)				
Category	AISI type 316 stainless steel		AISI type 316L stainless steel [23]	
	As-aged	Strauss tested	As-aged	Strauss tested
Not affected	0.00–0.015	0.00–0.27	0.00–0.1	0.0–0.3
Fissured	0.15–0.17	0.62–0.82	0.15–0.2	1.0–1.5
Cracked	0.21–0.49	2.43–6.7	0.17–0.2	1.7–2.0
Broken	0.6–0.65	7.5–7.85	0.2–0.27	2.3–3.0

depletion of chromium in type 316L stainless steel vis-à-vis type 316 stainless steel with high carbon content used in the present study. The high carbon content in the present steel caused considerable depletion of chromium and molybdenum thus producing detectable change in the conductivity/permeability, leading to reliable detection and assessment of DOS and the propensity for IGC, even in the as-aged condition.

A very important application arising from the present study is that by knowing the EC signal amplitude for different category specimens, the propensity to and extent of IGC could be assessed without subjecting the specimens to bend test. The impact of this would be felt during monitoring of the stainless steel components in service by providing vital information on the initiation and progress of IGC/IGSCC in service. Also, eddy current testing could be used as a very reliable tool to ensure quality of fabrication against sensitisation. This would help fabricators and the users to guard against sensitisation, particularly in applications where fabrication costs are linked to DOS.

The values of DOS obtained by EPR technique, depth of attack measurements and eddy current amplitude were correlated with each other, as shown in Figs. 9–11. A polynomial behaviour is observed between EC amplitude and other DOS assessment parameters. The following were the correlations:

(1) For eddy current amplitude (ECA (V)) vs ratio of peak current densities (I_r/I_a (%)) from EPR tests (Fig. 9).
I_r/I_a (%) = 151.06 (ECA (V))^2 − 23.127 (ECA (V)) + 0.534; R^2 = 0.9548—in as-aged condition.
I_r/I_a (%) = 1.444 (ECA (V))^2 − 6.1969 (ECA (V)) + 2.441; R^2 = 0.8863—after Strauss test.
(2) For ECA (V) vs ratio of charges (Q_r/Q_a (%)) from EPR tests (Fig. 10).
Q_r/Q_a (%) = 191.97 (ECA (V))^2 − 23.102 (ECA (V)) + 0.421; R^2 = 0.9699—as-aged condition.
Q_r/Q_a (%) = 1.6196 (ECA (V))^2 − 5.9619 (ECA (V)) + 2.818; R^2 = 0.8706—after Strauss test.
(3) For ECA (V) vs depth of attack (DOA (μm)) obtained from metallography.
DOA (μm) = 1197.7 (ECA (V))^2 − 672.87 (ECA (V)) + 190.54; R^2 = 0.7298—as-aged specimens.

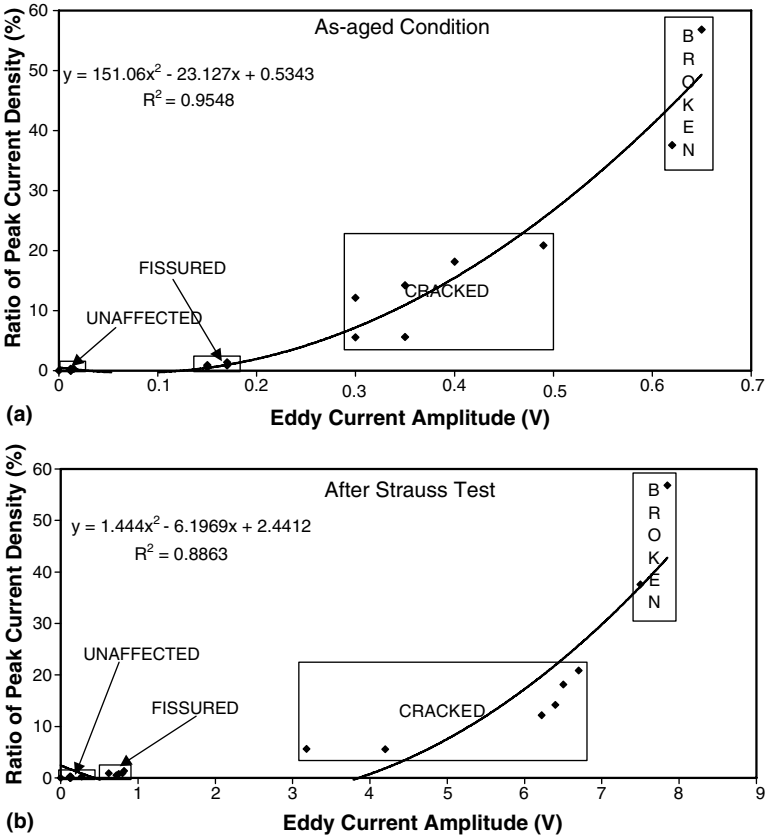

Fig. 9. Relationship between eddy current amplitude and ratio of peak current density: (a) as-aged condition and (b) Strauss tested condition.

DOA (μm) = 13.87 (ECA (V))^2 − 113.06 (ECA (V)) + 288.92; $R^2 = 0.7806$—after Strauss test.

The correlation of values of eddy current amplitudes with the various EPR assessment parameters has a higher R^2 value as compared to the correlation with the depth of attack. In the correlation of values of eddy current amplitudes with the various EPR assessment parameters, the correlation involving eddy current amplitude values of as-aged specimen gave better R^2 values. The significance of these empirical relationships is that knowledge of the eddy current amplitudes would help predict with some degree of confidence the DOS and the depth of attack that would have occurred during service of the component, thus helping in assessing the integrity of the component. However, for this to be feasible, proper optimisation of EC test parameters, precise calibrations and systematic and reliable measurements are important pre-requisites.

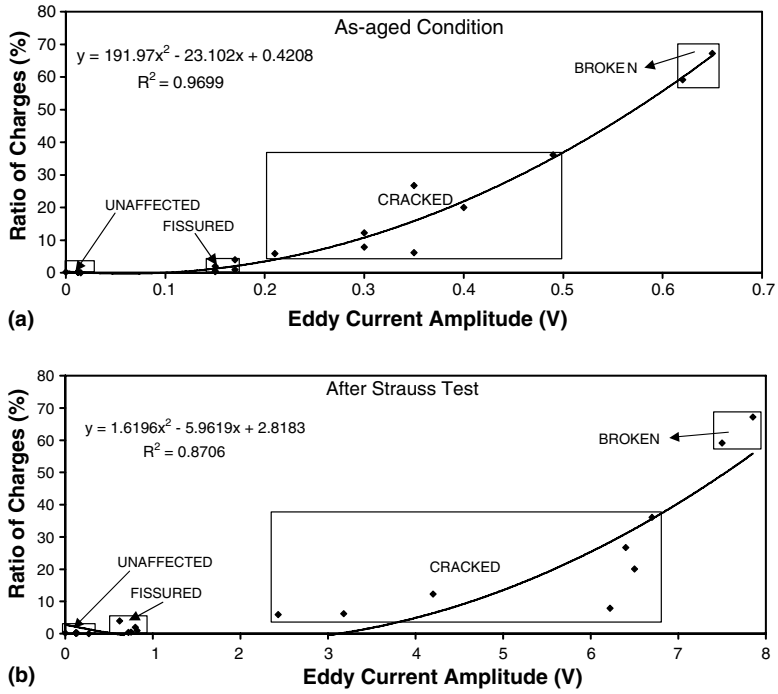

Fig. 10. Dependence of ratio of charge during reactivation to activation on eddy current amplitude: (a) as-aged condition and (b) after Strauss test.

4. Conclusions

AISI Type 316 stainless steel was subjected to various heat treatments between 873 and 1073 K for various durations of time. The aged specimens were then subjected to ASTM A262 Practice E test (accelerated Strauss test) in a boiling 16% H_2SO_4 solution containing 100 g/L of $CuSO_4 \cdot 6H_2O$ for 24 h and followed by a bend test. Based on the appearance at the bend portion, the specimens were classified into four categories viz. unaffected, fissured, cracked and broken. Electrochemical potentiokinetic reactivation technique was used to determine the DOS for the various categories of specimens. Eddy current tests were carried out to determine the eddy current amplitudes for the various categories of specimens in both the as-aged and Strauss-test exposed condition. It was possible to predict DOS in the as-aged conditions. However, the values of the EC amplitudes were much higher in the case of specimens after exposure to Strauss test. The reliable response of the eddy current amplitude to various changes in chromium depletion suggested it to be a good parameter to monitor the DOS and hence, the propensity for IGC attacks. Depth of attack by the Strauss test solution was measured on as-polished cross-sections of all categories of specimens. Only specimens that showed cracking

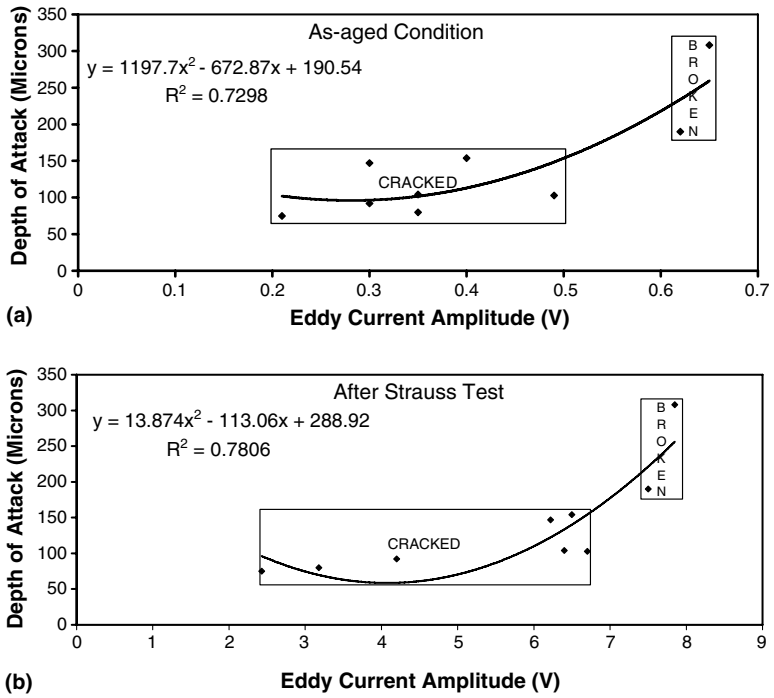

Fig. 11. Variation in depth of attack with changes in eddy current amplitude: (a) as-aged condition and (b) after Strauss test.

or were broken showed distinct attack by the Strauss test solution. Empirical relationships between eddy current amplitude and EPR parameters or depth of attack were established.

References

[1] D.G. Chakrapani, in: K.A. Esakul (Ed.), Handbook of Case Histories of Failure Analysis, ASM International, Metals Park, OH, 1992, p. 164.
[2] H.E. Ebert, in: K.A. Esakul (Ed.), Handbook of Case Histories of Failure Analysis, ASM International, Metals Park, OH, 1992, p. 278.
[3] S.M. Bruemmer, L.A. Charlott, Scripta Metallurgica 20 (1986) 1019.
[4] R.A. Mulford, E.L. Hall, C.L. Briant, Corrosion 39 (1983) 132.
[5] R.K. Dayal, J.B. Gnanamoorthy, Corrosion 36 (1980) 104.
[6] E. Folkhard, Welding Metallurgy of Stainless Steel, Springer-Verlag/Wien, 1988.
[7] T.A. Mozhi, W.A.T. Clarke, K. Nishimoto, W.B. John, D.D. McDonald, Corrosion 41 (1985) 555.
[8] N. Parvathavarthini, R.K. Dayal, J.B. Gnanamoorthy, Journal of Nuclear Materials 208 (1994) 251.
[9] N. Parvathavarthini, R.K. Dayal, S.K. Seshadri, J.B. Gnanamoorthy, Journal of Nuclear Materials 168 (1989) 83.
[10] S.M. Bruemmer, L.A. Charlott, B.W. Arey, Corrosion 44 (1988) 328.
[11] V. Kain, R.C. Prasad, P.K. De, H.S. Gadiyar, ASTM Journal of Testing and Evaluation 23 (1995) 50.
[12] A.J. Sedriks, Corrosion of Stainless Steels, John Wiley, New York, 1979.

[13] S.K. Mannan, R.K. Dayal, M. Vijayalakshmi, N. Parvathavarthini, Journal of Nuclear Materials 126 (1984) 1.
[14] ASTM Standard A262-93a, ASTM Book of Standards, American Society for Testing of Metals, Philadelphia, PA, 1993, p. 42.
[15] P. Muraleedharan, Corrosion and Maintenance (1984) 47.
[16] V. Cihal, Corrosion Science 20 (1980) 737.
[17] P. Novak, R. Stefec, F. Franz, Corrosion 31 (1975) 344.
[18] W.L. Clarke, W.M. Romero, J.C. Danko, Report GEAP-21382, GEC, California, 1976.
[19] ASTM Standard G 108-94, ASTM Book of Standards, American Society for Testing of Metals, Philadelphia, PA, 1994, p. 444.
[20] W.L. Clarke, J.R. Kearns, J.Y. Park, D. van Rooyen, ASTM Research Report, Subcommittee G01.08, 1989.
[21] P. Muraleedharan, J.B. Gnanamoorthy, K. Prasad Rao, Corrosion 45 (1989) 142.
[22] P. Ahmedabadi, V. Kain, P.R. Singh, P.K. De, Journal of Materials Engineering and Performance 12 (2003) 529.
[23] H.L. Libby, Introduction to Electromagnetic Nondestructive Testing Methods, Wiley Interscience, New York, 1971.
[24] H. Shaikh, B.P.C. Rao, S. Gupta, R.P. George, S. Venugopal, B. Sasi, T. Jayakumar, H.S. Khatak, British Corrosion Journal 37 (2002) 129.
[25] H. Shaikh, H.S. Khatak, J.B. Gnanamoorthy, Werkstoffe und Korrosion 38 (1987) 183.
[26] P. Muraleedharan, J.B. Gnanamoorthy, P. Rodriguez, Corrosion 52 (1996) 790.
[27] T.P.S. Gill, PhD Thesis, Indian Institute of Technology, Madras, India, 1984.
[28] F.C. Hull, Welding Journal 52 (1973) 104-s.
[29] International Standards Organisation, Technical Committee 156: Corrosion of Metals and Alloys, Working Group 9: Corrosion Testing of Materials for Power Generation: Revised Committee Draft ISO/CD 12372 for a Proposed Standard on Method for Electrochemical Potentiokinetic Reactivation Test, Seventh Revised Version, February, 1998.
[30] E.L. Hall, C.L. Briant, Metallurgical Transactions 15A (1984) 793.
[31] R.L. Cowan, C.S. Tedmon, Advances in Corrosion Science and Technology, vol. 3, Plenum Press, New York, 1973, p. 293.
[32] K. Mumtaz, S. Takahashi, J. Echigoya, L.F. Zhang, Y. Kamada, M. Sato, Journal of Materials Science Letters 21 (2002) 1199.

Glossary of acronyms

CCS: continuous cooling sensitisation
Cr^{eff}*:* effective Cr contents
DOS: degree of sensitisation
EC: eddy current
ECC: equivalent chromium content
ECT: eddy current testing
EPR: electrochemical potentiokinetic reactivation
HAZ: heat-affected zone
I_a*:* peak current density during activation
I_r*:* peak current density during reactivation
IGC: intergranular corrosion
IGSCC: intergranular stress corrosion cracking
ISO: International Standards Organisation
NECC: normalised equivalent chromium content
Q_a*:* activation charge
Q_r*:* reactivation charge
SCE: saturated calomel electrode
TTS: time–temperature-sensitisation